FEMS Microbiology Ecology, 97, 2021, fiab155

https://doi.org/10.1093/femsec/fiab155
Advance Access Publication Date: 26 November 2021
Research Article

RESEARCH ARTICLE

Temperature dependence of nitrate-reducing Fe(II) oxidation by *Acidovorax* strain BoFeN1 – evaluating the role of enzymatic vs. abiotic Fe(II) oxidation by nitrite

Nicole Dopffel[1,2,†], James Jamieson[3,4,*,†,‡], Casey Bryce[5], Prachi Joshi[2], Muammar Mansor[2], Adam Siade[3,4], Henning Prommer[3,4] and Andreas Kappler[2,6]

[1]Norwegian Research Center – NORCE, 22 Nygårdstangen, 5838 Bergen, Norway, [2]Geomicrobiology, Center for Applied Geosciences, University of Tübingen, 72074 Tübingen, Germany, [3]School of Earth Sciences, University of Western Australia, 35 Stirling Highway, 6009 Crawley, Australia, [4]CSIRO Land and Water, 147 Underwood Avenue, 6014 Floreat, Australia, [5]School of Earth Sciences, University of Bristol, Queens Road, Bristol BS8 1RJ, United Kingdom and [6]Cluster of Excellence EXC 2124: Controlling Microbes to Fight Infection, University of Tubingen, 72074 Tübingen, Germany

*Corresponding author: University of Western Australia, 35 Stirling Highway, 6009 Crawley, Australia. E-mail: james.jamieson@uwa.edu.au

One sentence summary: This study investigates chemical and microbially catalyzed Fe(II) oxidation across a range of temperatures to develop a quantitative description of enzymatic Fe(II) oxidation coupled to nitrate reduction within the environment.

†Both authors contributed equally to this publication.

Editor: Tillmann Lueders

‡James Jamieson, https://orcid.org/0000-0002-6161-5020

ABSTRACT

Fe(II) oxidation coupled to nitrate reduction is a widely observed metabolism. However, to what extent the observed Fe(II) oxidation is driven enzymatically or abiotically by metabolically produced nitrite remains puzzling. To distinguish between biotic and abiotic reactions, we cultivated the mixotrophic nitrate-reducing Fe(II)-oxidizing *Acidovorax* strain BoFeN1 over a wide range of temperatures and compared it to abiotic Fe(II) oxidation by nitrite at temperatures up to 60°C. The collected experimental data were subsequently analyzed through biogeochemical modeling. At 5°C, BoFeN1 cultures consumed acetate and reduced nitrate but did not significantly oxidize Fe(II). Abiotic Fe(II) oxidation by nitrite at different temperatures showed an Arrhenius-type behavior with an activation energy of 80±7 kJ/mol. Above 40°C, the kinetics of Fe(II) oxidation were abiotically driven, whereas at 30°C, where BoFeN1 can actively metabolize, the model-based interpretation strongly suggested that an enzymatic pathway was responsible for a large fraction (ca. 62%) of the oxidation. This result was reproduced even when no additional carbon source was present. Our results show that at below 30°C, i.e. at temperatures representing most natural environments, biological Fe(II) oxidation was largely responsible for overall Fe(II) oxidation, while abiotic Fe(II) oxidation by nitrite played a less important role.

Keywords: Fe oxidation; nitrate reduction; biogeochemical modeling; chemodenitrification

Received: 10 August 2021; **Accepted:** 24 November 2021

INTRODUCTION

Iron is a highly abundant, redox-sensitive element in the Earth's crust that can be used by a variety of microorganisms to gain energy (Kappler & Straub 2005; Kendall *et al.* 2012). Biogeochemical cycling of iron between its two main redox states Fe(III) and Fe(II) plays a crucial role for many processes in the environment, including greenhouse gas formation and the behavior of nutrients and toxic metal(loid)s (Borch *et al.* 2010; Kappler *et al.* 2021). At neutral pH, Fe(II) is readily oxidized by molecular oxygen, therefore the only viable pathways for microorganisms to live by Fe(II) oxidation is to grow under either acidic, microoxic or anoxic conditions (Hedrich, Schlomann and Johnson 2011). Under neutrophilic and anoxic conditions, some bacteria can couple Fe(II) oxidation to nitrate reduction (Straub *et al.* 1996). These so-called nitrate-reducing, Fe(II)-oxidizing bacteria have been isolated from a variety of different environments (Benz, Brune and Schink 1998). However, with only a few known exceptions (He *et al.* 2016; Laufer *et al.* 2016; Huang *et al.* 2021; Jakus *et al.* 2021), most of the strains have been shown to be mixotrophic and require an additional carbon source such as acetate for growth (Weber *et al.* 2006; Blöthe & Roden 2009; Bryce *et al.* 2018).

Reactive intermediates formed during heterotrophic denitrification include nitrite and nitric oxide, which are known to oxidize Fe(II) abiotically (Bonner & Pearsall 1982; Sorensen & Thorling 1991):

$$NO_3^- \rightarrow NO_2^- \rightarrow NO \rightarrow N_2O \rightarrow N_2 \quad (1)$$

While generally the reaction between nitrite and Fe(II) is relatively slow at neutral pH, reaction rates have shown to be significantly faster when catalytic surfaces such as iron minerals or cells are present (Coby & Picardal 2005; Tai & Dempsey 2009). These abiotic reactions may play a very important role for the metabolic functions of Fe(II)-oxidizing cultures as they could potentially cause complete Fe(II) oxidation without any direct enzymatic Fe(II)-oxidizing cell activity.

Ultimately, the question of whether mixotrophic nitrate-reducing Fe(II)-oxidizing strains are indeed capable of harvesting electrons and to gain energy from Fe(II) oxidation is still unresolved. Several studies have attempted to identify specific genes or proteins for Fe(II) oxidation in mixotrophic strains but failed to find any evidence for a cytochrome-like protein involved in electron transfer (Beller *et al.* 2013; Carlson *et al.* 2013). Jamieson *et al.* (2018) recently used process-based numerical modeling as an alternative tool to decipher and quantify the respective contributions of biotic and abiotic oxidation pathways of Fe(II) and found reactions with the intermediary NO_2^- to be significant for several bacterial strains. The simulated results found that at 25°C, ca. 25%–40% of the overall Fe(II) oxidation could be attributed to chemical denitrification by Fe(II), i.e., chemodenitrification. Similarly, Liu *et al.* (2019) found that chemodenitrification was a significant contributor to Fe(II) oxidation within Fe(II)-NO_3 systems for strain BoFeN1 and *Pseudogulbenkiania sp.* strain 2002. Importantly, Liu *et al.* (2019) found direct evidence that oxidized c-type cytochromes within extracellular polymeric substances, secreted by strains such as BoFeN1 when Fe(II) is present, were capable of oxidizing Fe(II), thus demonstrating a potential pathway for electron uptake. Further support for the significance of the abiotic chemodenitrification pathway is provided by the fact that the nitrate-reducing Fe(II)-oxidizing strain *Acidovorax* strain BoFeN1 is unable to oxidize Fe(II) when coupled to N_2O reduction (Klueglein & Kappler 2013). Fe(II) oxidation coupled to N_2O reduction, however, would only be expected if Fe(II) oxidation by strain BoFeN1 was coupled to all denitrification steps.

A metabolic oxidation of Fe(II) has been inferred for the same strain, due to a higher cell yield when cultivated in the presence of Fe(II) (Muehe *et al.* 2009). However, higher cell numbers were also observed in the presence of Fe(III), suggesting that Fe might act as a nutrient rather than an energy source (Klueglein & Kappler 2013). Contradictory to those results, other nitrate-reducing Fe(II)-oxidizing strains did not show higher cell numbers with Fe(III) (Chakraborty & Picardal 2013). In a study using *Acidovorax* strain 2AN, an enzymatic induction of Fe(II) was observed (Chakraborty & Picardal 2013), while this was not observed in cultures of *Acidovorax ebreus* (Carlson *et al.* 2013).

In this study, we explore the role of enzymatic activity in Fe(II) oxidation by strain BoFeN1 through a novel combined experimental and numerical modeling approach that exploits two well-established (bio)geochemical relationships. First, the rate of abiotic (chemical) reactions is known to increase logarithmically with increasing temperatures (T), closely following a linear relationship between rate constant [ln(*k*)] and 1/T, as described by the Arrhenius equation (Laidler 1984). Second, microbially catalyzed reactions show a distinctly different relationship between reaction rates and temperatures to what would be expected from typical Arrhenius kinetics. Reaction rates are typically fastest for a strain-specific optimal temperature, while decreasing at temperatures above and below that optimum, as described by the Ratkowsky equation (Ratkowsky *et al.* 1982). Depending on the strain, cells will still be metabolically active over a broad temperature range outside their optimum temperature, which is also the case for Fe(II)-oxidizers. For example, Ahonen and Tuovinen (1989) showed that the acidophilic Fe(II)-oxidizer *Thiobacillus ferrooxidans* is capable of oxidizing iron over a temperature range from 4–38°C, but shows a seven-fold decrease in growth rate from the rate within the optimal temperature range of 25–35°C. Furthermore, Vollrath *et al.* (2013) showed that the microaerophilic Fe(II)-oxidizer *Leptrotrix cholodnii* is able to compete with the abiotic Fe(II) oxidation by oxygen at temperatures between 11°C and 37°C.

Here, we hypothesize that the differing temperature-dependencies of abiotic vs. biotic reaction pathways will allow us to more reliably determine the contribution of enzymatic oxidation processes compared to previous studies investigating these pathways at a single temperature. For this study, we use the strain *Acidovorax* BoFeN1, which has previously been shown to have the ability to grow in conjunction with nitrate reduction over a wide temperature range from 4°C to 37°C (Muehe *et al.* 2009). By performing Fe(II) oxidation experiments at varying temperatures and taking into account the established temperature characteristics of both pathways, we assess the varying biotic and abiotic contributions to Fe(II) oxidation at different temperatures. The obtained experimental data were subsequently analyzed through a process-based modeling approach, which provides us with a quantitative description of enzymatic Fe(II) oxidation coupled to nitrate reduction over a broad range of environmentally relevant temperatures.

MATERIAL AND METHODS

Source of microorganism

Acidovorax strain BoFeN1 is a chemoorganotrophic, nitrate-reducing Fe(II)-oxidizing bacterium that was originally isolated from Lake Constance sediments and has been kept in the authors' laboratory since then (Kappler, Schink and Newman 2005).

Microbial growth media and growth conditions

For routine cultivation of strain BoFeN1, 10 mM Na-nitrate and 5 mM Na-acetate were added to a 22 mM bicarbonate-buffered low phosphate mineral medium (pH 7.1), which was prepared anoxically, as described earlier (Hegler *et al.* 2010) and incubated at 28°C. For the oxidation experiments in this study, media containing ∼8 mM of dissolved Fe(II) were prepared as previously described by Klueglein and Kappler (2013).

Medium pre-filtration

As standard procedure, the medium was filtered (0.22 μm) after addition of 10 mM of Fe(II) but before addition of acetate, nitrate or microbes. This was done to remove Fe(II) phosphate and Fe(II) carbonate minerals, which form in the media and could act as catalytic surfaces for the investigated reactions. For abiotic controls aimed at testing the effect of organic-rich nitrite-containing culture fluids without cells, some inoculated bottles were again sterile-filtered (0.22 μm). The only instance where the medium was not filtered were the experiments in which the cells were first cultured without Fe(II), and Fe(II) was added during growth. Therefore, in these setups the neo-formed Fe(II) minerals could not be removed (Fig. 1).

Experimental setup—enzymatic and abiotic Fe(II) oxidation at different temperatures under mixotrophic conditions

To evaluate the relative importance of abiotic versus biotic reactions, the capacity of BoFeN1 to grow at low temperatures in the presence of Fe(II) while accumulating high concentrations of nitrite was exploited. Bottles were initially filled anoxically with 25 mL of Fe(II)-containing, pre-filtered medium and amended with anoxic 10 mM Na-nitrate and 5 mM Na-acetate. Thereafter, the bottles were inoculated with 4% (v/v) (ca. 5×10^6 cells/ml) of a four-day old pre-culture grown at 28°C on 5 mM acetate and 10 mM nitrate. Replicate bottles were incubated at 5, 13, 20 or 28°C in order to test the effect of temperature on BoFeN1 growth, Fe(II) oxidation and nitrite accumulation.

Cultures incubated at 5°C were chosen for subsequent experiments due to positive growth of BoFeN1 coupled to limited oxidation of Fe(II) by chemodenitrification due to the very slow abiotic kinetics at this low temperature. After growth of BoFeN1 for 10–15 days at 5°C, the nitrite concentration was quantified and replicate incubations were heated to different temperatures by transferring the bottles into heated water baths with temperatures set to either 30, 40, 50 or 60°C (enzymatic temperature dependent Fe(II) oxidation, Fig. 1). In parallel, organo-nitrite controls were set up by inoculating filtered (0.22 μm, mixed cellulose esters, Millipore) aliquots of the 5°C pre-culture into replicate bottles (Fig. 1). The purpose of the organo-nitrite controls was to investigate if culture fluids (containing extracellular organics) can influence the rate of Fe(II) oxidation and nitrate reduction. For the abiotic Fe(II) oxidation by nitrite experiments (i.e., chemodenitrification), sterile bottles with pre-filtered medium were amended with different concentrations of Na-nitrite (temperature dependent chemodenitrification, Fig. 1).

Experimental setup—enzymatic and abiotic Fe(II) oxidation in the absence of organic carbon (starved cells)

To determine enzymatic Fe(II) oxidation compared to abiotic Fe(II) oxidation by nitrite in the absence of acetate (which leads to heterotrophic nitrate/nitrite reduction thus further influencing Fe(II) oxidation), BoFeN1 was first cultivated without Fe(II) but with 10 mM nitrate and 5 mM acetate at 13°C for approximately 5 days. An additional 10 mM of nitrate was added to the bottles after complete acetate consumption. An additional 5 days of incubation proceeded to starve the cells of all available stored carbon. No nitrite was produced under this condition—therefore, these experiments would not have been comparable to those where the cells were grown under mixotrophic conditions at 5°C (see previous section). Subsequently, 2 mM of nitrite was added to all bottles to mimic biological production of nitrite, followed by addition of ∼10 mM Fe(II). After Fe(II) addition, a whitish precipitate formed, indicating the formation of siderite and vivianite, as previously described by (Kappler and Newman 2004). Bottles were then heated to 30°C in a water bath (starved enzymatic Fe(II) oxidation, Fig. 1). As controls (organo-nitrite controls), a subset of bottles was sterile-filtered after Fe(II) addition and incubated at the same temperature (30°C). Fe(II) oxidation was followed over time. Once Fe(II) oxidation was complete, nitrite and nitrate were quantified once more.

Analytical methods

For the quantification of total Fe(II), i.e., the sum of dissolved and solid phase Fe(II), samples were diluted in 40 mM sulfamic acid to avoid abiotic Fe(II) oxidation by nitrite during acidification (Klueglein & Kappler 2013; Schaedler, Kappler and Schmidt 2018). A 100 μL aliquot of culture suspension was withdrawn anoxically with a syringe and dissolved in 900 μL sulfamic acid for 1 hour at room temperature. The ferrozine–Fe(II) complex was quantified at 562 nm using a microtiter plate reader (FlashScan 550, Analytik Jena, Germany). Each sample was measured in triplicate. Acetate was quantified by HPLC (Class vp with RID 10 A & DAD SPM 10 A vp detectors, Shimadzu, Japan; precolumn: Micro guard cation H cartridge; main column: Aminex HPX-87H Ion exclusion column 300 mm x 7.8 mm, Bio-Rad, Austria; eluent: 5 mM H_2SO_4 in MQ water). Cell growth in iron-free cultures was quantified by measuring optical density (OD) at 600 nm (SPEKOL 1300, Analytik Jena, Germany) in culture tubes. Nitrate and nitrite were quantified by a continuous flow analyzer system containing a dialysis membrane for iron removal to prevent side reactions of nitrite and nitrate during analysis (Seal Analytical, Norderstedt, Germany). In this automated system, nitrate is reduced to nitrite with hydrazine sulfate and quantified photometrically with N-1-naphtylethylendiamin at 550 nm. Minerals were identified with a μ-XRD-device (Bruker D8 Discover X-ray diffraction instrument, Bruker AXS GmbH, Germany) equipped with a Co K_α X-ray tube and operating at 30 kV/30 mA. The EVA® 10.0.1.0 software was used to identify the mineral

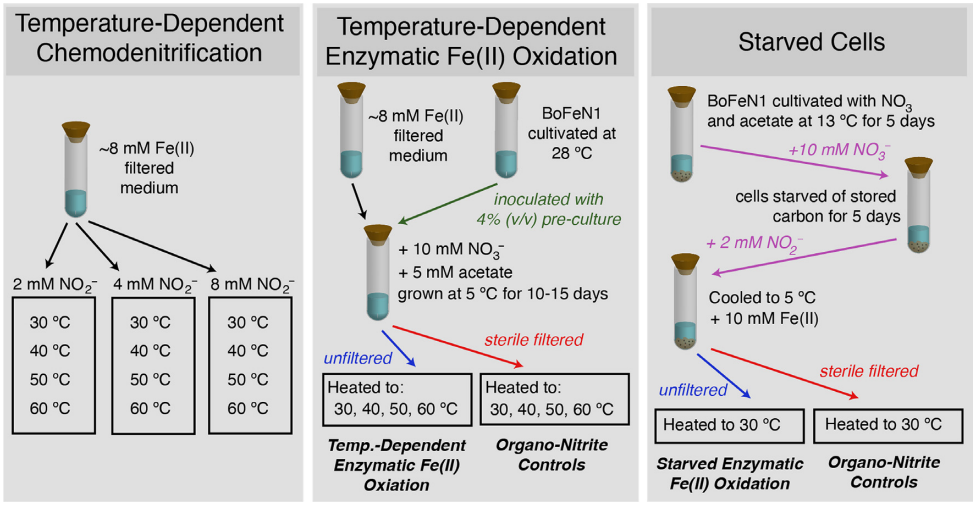

Figure 1. Schematic illustration of the experimental setup of the temperature-dependent (fully abiotic) chemodenitrification experiments (left), temperature-dependent enzymatic Fe(II) oxidation experiments (middle), and the starved cells experiments (right).

phases using the PDF-database licensed by ICDD (International Centre for Diffraction Data).

Rate calculation and Arrhenius plot

The oxidation rates of Fe(II) by NO_2^- were evaluated using a second order and zeroth order rate equation:

$$d\,[Fe\,(II)]\,/dt\; = -k_{obs}\left[Fe(II)_{aq}\right]\left[NO_2^-\right] \quad (2)$$

$$d\,[Fe\,(II)]\,/dt\; = -k_{obs} \quad (3)$$

where k_{obs} is the observed rate constant (L mol^{-1} sec^{-1} for Eq. 2 and mol L^{-1} s^{-1} for Eq. 3). The values for the zero-order derived k_{obs} were fitted into the Arrhenius equation to yield a slope to derive the activation energy (E_a) for Fe(II) oxidation by nitrite.

$$k = Ae^{-Ea/RT} \quad (4)$$

where k is the reaction rate constant (mol L^{-1} s^{-1}), A is the frequency factor (mol L^{-1} s^{-1}), R is the gas constant (J mol^{-1} K^{-1}) and T is temperature (K), respectively. An Arrhenius plot of ln(k) against 1/T therefore yields a line with the slope -E_a/R (Ahonen & Tuovinen 1989) where E_a is the activation energy (J mol^{-1}).

Microscopy

For Scanning Electron Microscopy (SEM), samples containing bacteria were centrifuged and washed with acetone once at the end of Fe(II) oxidation. The samples were mounted on a carbon grid; vacuum dried for several hours, coated with platinum and examined with a LEO Modell 1450 VP at 5 kV.

Process-based biogeochemical model simulations

A process-based biogeochemical model, implemented in PHREEQC3 (Parkhurst & Appelo 2013), was employed to interpret the experimental data collected in this study. The model was originally developed and applied to simulate the Fe(II) oxidation behavior observed in several different incubation studies (Jamieson *et al.* 2018), with each study using bacteria that were identified earlier as being capable of supporting nitrate-reducing Fe(II) oxidation. The reaction network assumed heterotrophic nitrate reduction to nitrite (Reaction 5) and nitrite reduction to nitrogen gas (Reaction 6).

$$CH_3COO^- + 4\,NO_3^- \rightarrow 4\,NO_2^- + H_2O + HCO_3^- + CO_2\,(g) \quad (5)$$

$$3\,CH_3COO^- + 8\,NO_2^- + 8\,H^+ \rightarrow 4\,N_2\,(g) + 7\,H_2O + 3\,HCO_3^- + 3\,CO_2\,(g) \quad (6)$$

The biological coupling of dissolved Fe(II) oxidation to nitrate reduction was assumed to produce nitrite (Reaction 7), while the consumption of solid-phase Fe(II) (e.g., siderite) by bacteria was assumed to be negligible (Weber, Picardal and Roden 2001). Nitrite produced from these reactions was assumed to abiotically react with Fe(II) to produce N_2O, as per Reaction 8. The rate of this reaction was quantified using Eq. 9 (Tai & Dempsey 2009):

$$2\,Fe\,(II) + NO_3^- + 2\,H^+ \rightarrow 2\,Fe\,(III) + NO_2^- + H_2O \quad (7)$$

$$4\,Fe\,(II) + 2\,NO_2^- + 5H_2O \rightarrow 4\,FeO\,(OH) + N_2O_{(g)} + 6\,H^+ \quad (8)$$

$$\frac{d\,[Fe\,(II)]}{dt} = -k_{ab}\left[Fe(II)_{aq}\right]\left[NO_2^-\right] \quad (9)$$

where k_{ab} is the rate constant (mol^{-2} sec^{-1}). A surface complexation model was used to quantify the loss of dissolved Fe(II) by adsorption onto neo-formed Fe minerals. Sorption site densities were calculated assuming 2.00 (Mathur & Dzombak 2006) and 11 sites nm^{-2} (Van Cappellen *et al.* 1993) for goethite and siderite, respectively. Equilibrium surface complexation constants for Fe(II) sorption were taken from (Hinkle *et al.* 2015) and (Pokrovsky & Schott 2002), respectively.

An empirical temperature-dependent growth rate constant was incorporated into the microbial respiration rate following the linear equation proposed by Rawkowski et al. (1983):

$$u = b\,(T - T_{min})\,\{1 - \exp\,[c\,(T - T_{max})]\} \quad (10)$$

where b and c were considered empirical fitting parameters in this study. While generally b is the regression coefficient of the square root of growth rate versus degrees Kelvin below the optimal growth temperature, this data was not available. T_{min} and T_{max} are the minimum and maximum temperatures, respectively, at which the growth rate is zero. These were assumed to be 1 and 40°C based on experimental evidence acquired in this

study, and were also consistent with previous work investigating the optimal growth conditions for strain BoFeN1 (Muehe et al. 2009).

The overall microbial respiration rate, v_{bio} (mol L^{-1} s^{-1}) is described by:

$$v_{bio} = k_{bio}\,[X]\,uF_D F_A F_T \quad (11)$$

where k_{bio} is a rate constant (mol (mol cells)$^{-1}$ s^{-1}), F_D and F_A are unitless kinetic factors, F_T is a unitless thermodynamic factor and X is the biomass concentration (mol L^{-1}), in accordance with the formulation proposed earlier by Jin and Bethke (2003). Additionally, the biomass growth was described by:

$$\frac{d\,[X]}{dt} = Y v_{bio} - D_e \quad (12)$$

where Y is the biomass yield coefficient (mol cells per mole acetate), v_{bio} is the microbial respiration rate (mol L^{-1} s^{-1}) and D_e was an encrustation inhibition term (mol L^{-1} s^{-1}) used to account for the cells becoming heavily encrusted in Fe minerals during incubation experiments (Jamieson et al. 2018). A factor of 10^{-13} g $cell^{-1}$ was used to convert from cells mL^{-1} to mol L^{-1} using the formula for biomass given a generic formula of $C_5H_7O_2N$.

Following Pantke et al. (2012), the Fe(III) produced from oxidation of Fe(II) was assumed to precipitate as the mixed-valent green rust carbonate ($[Fe^{2+}{}_4Fe^{3+}{}_2(HO^-)_{12}]^{2+} \cdot [CO^{2-}{}_3 \cdot 2H_2O]^{2-}$) before being further oxidized by NO_2^- (Pantke et al. 2012), thereby transforming it into the stable Fe(III) phase goethite. Alternatively, goethite could precipitate directly from solution. The precipitation of goethite was assumed to be kinetically controlled and to follow a rate law derived from transition-state-theory:

$$r_k = k_{goe}\,(1 - \Omega) \quad (13)$$

where r_k is the rate of precipitation in mol L^{-1} sec^{-1}, k_{goe} is the precipitation rate constant (mol L^{-1} s^{-1}) and Ω is the saturation ratio. The oxidation of green rust by nitrite followed an overall first order kinetic rate law (Hansen et al. 1996):

$$\frac{d\,[NH_4^+]}{dt} = k_{gr\_t}\,[Fe(II)_{GR}] \quad (14)$$

where k_{gr_t} was adjusted for temperature according to (Palandri & Kharaka 2004):

$$k_{gr\_t} = 10^{\log(k_{grox}) - \left(\frac{E_a}{2.303 \times 8.314}\right) \times \left(\frac{1}{Tk} - \frac{1}{298.15}\right)} \quad (15)$$

where the rate constant k_{grox} was equal to 2.07×10^{-5} mol L^{-1} sec^{-1}, slightly adjusted from the calibrated value reported by Jamieson et al. (2018). The activation energy employed in Eq. 15 was 83.9 kJ mol^{-1} (Hansen & Koch 1998) and *Tk* is the temperature (K). The reduction of nitrite in this reaction was assumed to produce ammonium (Etique et al. 2014). Additionally, the precipitation of siderite was included, based on previous experimental work that suggested that this mineral phase formed after the addition of Fe(II) to the bicarbonate rich culture medium (Pantke et al. 2012). The precipitation rate of siderite was modeled using the reaction rate formulation presented by Sun and Nešić (2008), amended with the temperature dependence term proposed by Greenberg and Tomson (Greenberg & Tomson 1992).

$$r_{sid,ppt} = k_{sid} e^{\frac{-\Delta G_a}{RT}} K_{sp,T,}\,(\Omega - 1) \quad (16)$$

where k_{sid} is the precipitation rate constant, ΔG_a is the surface activation energy (73.7 kJ mol^{-1}) and K_{sp} is the solubility product that includes the effects of temperature according to the modified expression proposed by Jiang and Tosca (2020):

$$\log K_{sp,T} = -58.6989 - 0.041377T - \frac{2.196}{T} + 24.5724 \log T \quad (17)$$

A full description of the development and previous application of the biogeochemical modeling framework is provided in Jamieson et al. (2018).

The parameterization of the biogeochemical model used in this study was largely adapted from that used in Jamieson et al. (2018) for strain BoFeN1, with a few minor exceptions that were required due (i) to the introduction of new processes and (ii) variations in the rate expressions to reflect new insights generated during this study, including the empirical temperature-dependent growth constant, siderite precipitation, recalibrated chemodenitrification kinetics to account for temperature effects and data collected within this study.

The model calibration involved a total of 5 adjustable parameters and was performed with the software package PEST++ (Welter et al. 2015). These 5 parameters included (i) rate constants for siderite precipitation, (ii) chemodenitrification, (iii) nitrite reduction at 5°C and 13°C and (iv) the activation energy for chemodenitrification. Where possible, initial parameter estimates were taken from the previously published model and adjusted to their equivalent value after including the relevant Arrhenius terms in the rate expression. The initial estimate for the chemodenitrification activation energy was the calculated average derived from all triplicate experiments across all the investigated temperature ranges. During model calibration this parameter value could deviate by the calculated standard deviation. The sum of squared residuals between 344 observations and their associated model simulated results were used as the objective function during the calibration procedure. Table S1 (Supporting Information) provides a summary of all employed model parameters and initial conditions for the model simulations.

RESULTS

Abiotic Fe(II) oxidation by nitrite at different temperatures

As a first step, temperature dependent (fully abiotic) chemodenitrification was characterized for our specific microbial growth medium. We measured Fe(II) oxidation by nitrite over time at four different temperatures (30, 40, 50 and 60°C) after addition of three biologically relevant nitrite concentrations (2, 4 and 8 mM) to pre-filtered medium containing ~8 mM of dissolved Fe(II) (Fig. 2). The measured Fe(II) oxidation rates for all abiotic and biotic experiments are presented in Table S2 (Supporting Information). Shortly after nitrite addition to the Fe(II)-amended medium, a green mineral phase formed, most likely the mixed Fe(II)/(Fe(III) mineral green rust (Fig. S1, Supporting Information). Fe(II) oxidation was very fast at higher temperatures whereby the Fe(III) mineral goethite formed as the main reaction product in all setups, as analyzed by XRD (Fig. S2, Supporting Information). The apparent rates of Fe(II) oxidation by NO_2^- were initially evaluated by the integrated rate equation following Tai & Dempsey (2009):

$$k_{obs}t = \frac{1}{[Fe(II)_{diss}]_0 - 2[NO_2^-]_0} \mathrm{Ln} \frac{[NO_2^-]_0\,([Fe(II)_{diss}]_0 - x)}{[Fe(II)_{diss}]_0\,([NO_2^-]_0 - 0.5x)} \quad (18)$$

However, the kinetics of the set of experiments performed with 2 mM of nitrite could not be resolved using this equation as the extent of Fe(II) loss exceeded the stoichiometric amount that could have been oxidized based on the amount of oxidant (i.e. nitrite) that was added. The total amount of Fe(II) lost was between 161% and 195% of the amount of nitrite added, according to Reaction 8, robably due to sorption to or precipitation at

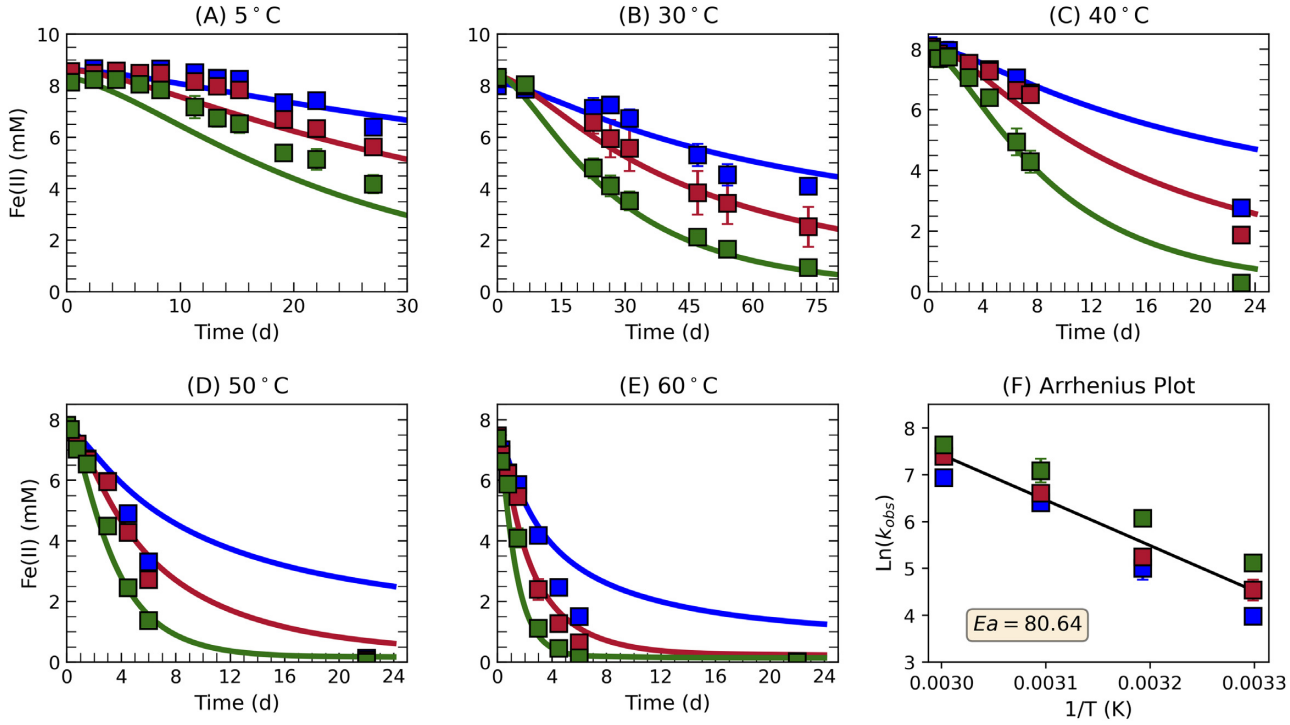

Figure 2. Results of chemodenitrification experiments (using pre-filtered medium) at either 2, 4 or 8 mM nitrite concentrations at temperatures of 5, 30, 40, 50 and 60°C (panels **A to E**). Experimental results (symbols) and simulation results (solid line) are presented for total Fe(II) concentrations. Model simulations include the loss of Fe(II) by precipitation of siderite and sorption. **(F)** Arrhenius plot of abiotic Fe(II) oxidation rates by nitrite at pH 7. The slope of the regression line yields the activation energy with $E_a = 80 \pm 7$ kJ/mol. Data for the Arrhenius plot is taken from the linear-least squares fit of Fe(II) observations within the first 24 hrs for each experiment. Each symbol represents the mean value of an independent experiment with duplicates conducted at different temperatures.

the glass wall (see discussion). Consequently, only Fe(II) data collected either within 24 hours for experiments conducted at 30°C or within 6 hours for all other temperatures and nitrite concentrations were used for the determination of k_{obs}, where the loss of Fe(II) from processes other than chemodenitrification are less pronounced. For all considered experiments, at least four concentration and time data points were included in the determination of the rate constant. The rates were observed to be zeroth order and ranged from 54 to 2068 μM h^{-1} for 2 mM nitrite at 30°C and 8 mM at 60°C, respectively, and showed typical Arrhenius-like behavior with a linear slope for the investigated temperature range from 30–60°C, yielding an activation energy of 80±7 kJ/mol (Fig. 2(F)). The measured chemical reaction between nitrite and Fe(II) is very slow at 5°C (Fig. 2(A)).

Growth and Fe(II) oxidation by BoFeN1 at 5, 13, 20 and 28°C

The experiments with BoFeN1 at 5°C showed that the strain was still able to grow in response to the addition of 10 mM nitrate and 5 mM acetate (no Fe(II)), thereby reaching a maximum OD_{600} value of ~0.15 at day 9 after an initial lag phase of approximately 4 days (Fig. 3E). In contrast, at the strain's temperature optimum of 28°C, a max. OD_{600} of 0.2 was reached within ~2 days. When BoFeN1 was inoculated with additional 8 mM Fe(II), we observed only very little Fe(II) oxidation at 5°C (Fig. 3A). At 28°C, all Fe(II) was oxidized to Fe(III) within 5 days. Acetate consumption was very slow at 5°C and at the end of the experiment, i.e. after 14 days, 2.6±0.9 mM acetate remained in solution (Fig. 3). At 28°C, all available acetate was consumed within 2 days. Low temperature setups containing Fe(II), acetate and nitrate, resulted in the accumulation of high concentrations of nitrite of up to 3.7±0.1 mM after 14 days, while only 1.1 mM nitrite accumulated in the cultures growing at 28°C (Fig. 3).

Comparison of abiotic and biotic Fe(II) oxidation rates at different temperatures

Enzymatic temperature dependent Fe(II) oxidation experiments were compared using incubations conducted at the same temperatures as the temperature dependent chemodenitrification experiments (30, 40, 50 and 60åC after 10 to 15 days of growth at 5åC). Fig. 4 shows the observed Fe(II) oxidation rates for enzymatic temperature dependent Fe(II) oxidation experiments, plotted against the chemodenitrification oxidation rates. At 50°C and 60°C the Fe(II) oxidation rates observed for the enzymatic Fe(II) oxidation experiments and the organo-nitrite control experiments were both in the range of the calculated chemodenitrification Fe(II) oxidation rates, consistent with a purely abiotic reaction between Fe(II) and nitrite (Fig. 4). At the upper limit of the strain's capability to grow (40°C), the measured Fe(II) oxidation rates also remained in the range of the calculated chemodenitrification rates (Fig. 4). At 30°C, however, the enzymatic Fe(II) oxidation experiments containing strain BoFeN1 showed higher Fe(II) oxidation rates compared to the organo-nitrite controls and chemodenitrification experiments (Fig. 4). Interestingly, the oxidation rates within organo-nitrite controls were also marginally higher than the equivalent abiotic experiments. This could potentially have been due to promotion of Fe(II) oxidation by the enzyme c-type cytochromes within EPS (Liu *et al.* 2019) that would still have been present in solution after sterile filtration.

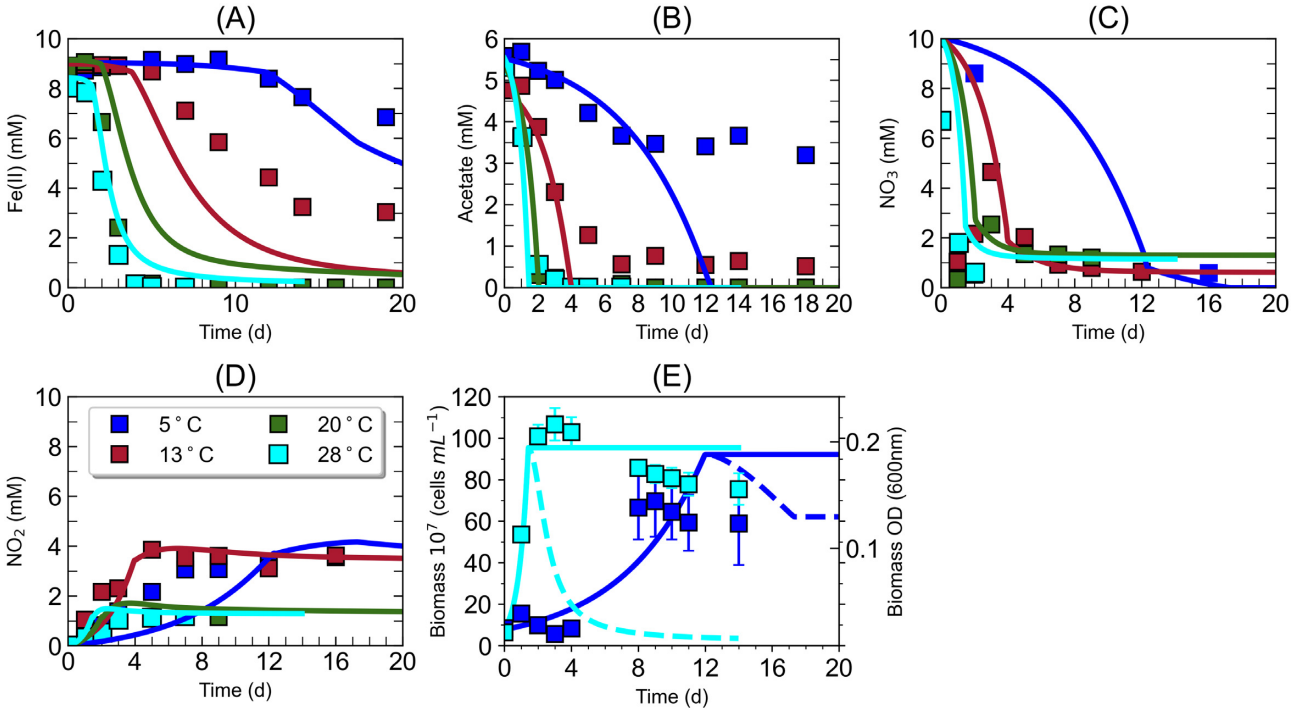

Figure 3. *Acidovorax* strain BoFeN1 cultivated with 5 mM acetate, 10 mM nitrate and ~8 mM Fe(II) at 5, 13, 20 and 28°C in pre-filtered medium. Symbols represent the measured data and solid lines represent the model results. Sterile controls showed no Fe(II) oxidation and no change in acetate or nitrite concentration (not shown). Error bars respresent mean values of two independent experiments. Absence of error bars indicate error was smaller than symbol size. Optical density (OD_{600nm}) measurements over time of cultures of *Acidovorax* strain BoFeN1 cultivated with 10 mM nitrate and 5 mM acetate at 28 or 5°C. Model results are given as biomass in 10^7 cells mL^{-1} (a factor of 10^{-13} g $cell^{-1}$ was used to convert from cells mL^{-1} to mol L^{-1} using the formula for biomass given a generic formula of $C_5H_7O_2N$). Dashed lines represent biomass subject to encrustation whereas the solid line represents uninhibited biomass for reference. Error bars indicate standard deviation of triplates. Absence of error bars indicate error was smaller than symbol size.

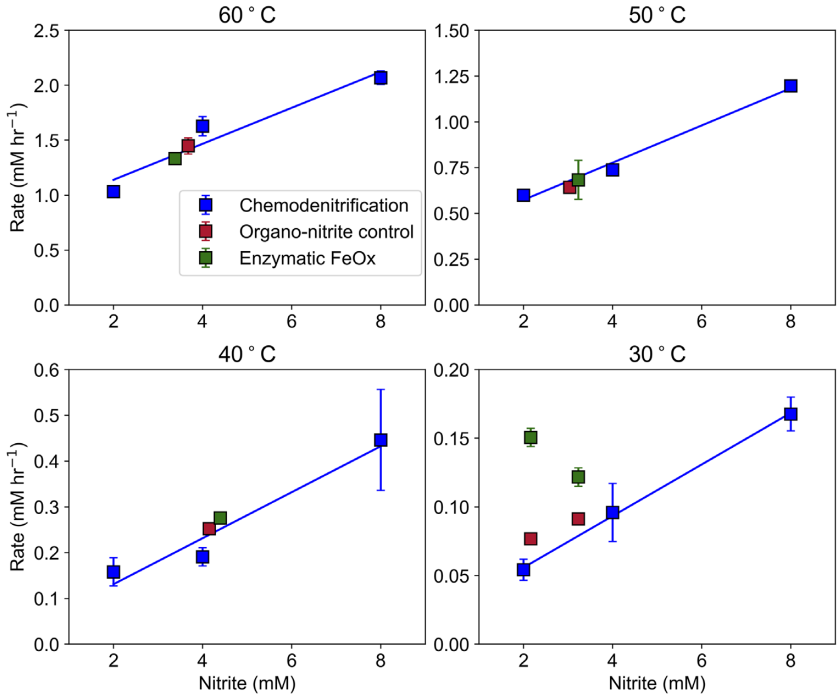

Figure 4. Measured Fe(II) oxidation rates (zero-order k_{obs}, as provided in Table S1, Supporting Information) plotted against the nitrite concentrations evaluated in this study at different temperatures (using pre-filtered medium). Blue squares are chemodenitrification Fe(II) oxidation rates. Green squares are oxidation rates within the enzymatic Fe(II) oxidation cultures of *Acidovorax* strain BoFeN1, initially cultivated with 10 mM nitrate, 5 mM acetate and ~ 8 mM Fe(II) for 10–15 days at 5åC before heat treatment at 30, 40, 50 or 60åC. Red squares are organo-nitrite controls that were sterile filtered. Every symbol represents an independent experiment with triplicates and error bars are the standard deviation.

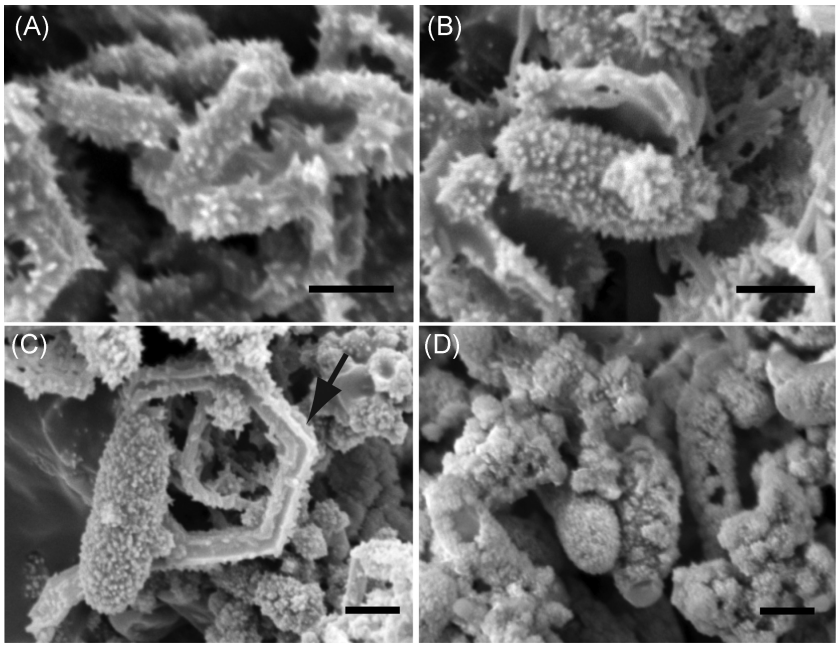

Figure 5. SEM images of encrusted cells of *Acidovorax* strain BoFeN1 after incubation for 1–5 days at 60°C **(A)**, 50°C **(B)**, 40°C **(C)** and 30°C **(D)** with accumulated nitrite present after 10–14 days incubation at 5°C with 10 mM nitrate, 5 mM acetate and ~8 mM Fe(II). Arrow points to a hexogonal mineral ring. Scale bars are 1 μm.

However, a complicating factor in the interpretation of the results obtained for the enzymatic Fe(II) oxidation experiment performed at 30°C was that significant residual amounts of nitrate and acetate remained at the end of the 5°C incubation period. This leads to additional nitrite production during the experiment conducted at 30°C due to continued biological denitrification (Fig. 3). This was not the case for the experiments at higher temperatures as the strain BoFeN1 is not active at temperatures above 40°C.

To minimize the impact of continuous heterotrophic denitrification on the results, we starved the cells by cultivating BoFeN1 without iron at low temperatures (13°C) until all acetate was consumed. Subsequently, we added nitrate (10 mM) to induce consumption of cell-stored carbon. As BoFeN1 does not accumulate nitrite in the absence of Fe(II), 2 mM nitrite was added to the cultures, which then provided BoFeN1 with additional electron acceptor capacity (Muehe *et al.* 2009). After addition of both Fe(II) and 2 mM NO_2^-, the bottles were incubated at 30°C. Once again, we observed a significantly higher Fe(II) oxidation rate (Fig. 6) in the bottles containing starved cells of strain BoFeN1 (0.46±0.25 mM/h) compared to the organo-nitrite control bottles that were sterile-filtered (0.24±0.05 mM/h). After 55 hours, almost twice as much total Fe(II) was oxidized in the bottles containing starved cells (7.2 mM with BoFeN1) compared to the organo-nitrite controls (4.0 mM in sterile filtered setups). It should be noted that in these specific bottles the medium could not be filtered after Fe(II) addition, and we observed mineral precipitation after Fe(II) addition, which could influence overall reaction rates.

For all experiments, SEM imaging of BoFeN1 after Fe(II) oxidation showed the formation of encrusted cells with rod-shaped, globular and ring-shaped minerals, probably an initial formation of green rust at 40, 50 and 60°C (Fig. 5C, arrow and Fig. S3, Supporting Information) and some poorly-crystalline-ferrihydrite-type Fe(III) oxyhydroxides at lower temperatures and a terminal mineral phase of more needle-like goethite at higher temperatures (Pantke *et al.* 2012).

DISCUSSION

Temperature dependent chemodenitrification

The kinetics of abiotic Fe^{+2}_{diss} oxidation by nitrite are generally well described by the second-order rate expression, Eq. 9 (Tai & Dempsey 2009; Kopf, Henny and Newman 2013). However, apparent rate constants k_{obs} for second-order kinetics could not be determined for all temperature dependent chemodenitrification experiments (Fig. S4, Supporting Information), given the higher-than-expected loss of Fe(II). This implied the existence of either: (i) another unknown oxidant, such as oxygen, which was regarded as unlikely given the strict anoxic protocols; or (ii) other sinks of Fe(II), such as Fe(II) mineral precipitation or sorption of Fe(II) to glass walls (Notini *et al.* 2019). To prevent inclusion of data that were affected by processes other than Fe(II) oxidation, only data collected during the initial stages of the experiment were included and fitted by a linear-least squares fit to derive the apparent rate constants, k_{app}. This is in line with the findings of Kopf, Henny and Newman (2013), who suggested that when a strong ligand, such as citrate, was absent from a standard bicarbonate basal medium, the reaction between nitrite and Fe(II) appeared zeroth-order.

The Arrhenius plot of k_{app} derived from linear-least squares fits for each temperature yielded a linear relationship. The slope of the derived curve was used to calculate an activation energy of 80±7 kJ/mol at pH 7. This is in good agreement with the activation energy of 72.7–94.6 kJ/mol determined earlier by Van Cleemput and Baert (Van Cleemput & Baert 1983) for the reaction between nitrite and 10–16 mM Fe(II) at pH 6. In our study, we observed a typical Arrhenius-like behavior for the abiotic reaction between nitrite and Fe(II) at neutral pH with very slow rates at 5°C and high rates at 30°C–60°C (Fig. 2). The empirical relationship shows a temperature increase of 10°C to cause a doubling of the reaction rate.

The model-simulated results of the temperature dependent chemodenitrification experiments were generally well reproduced across all temperatures and nitrite concentrations (Fig. 2).

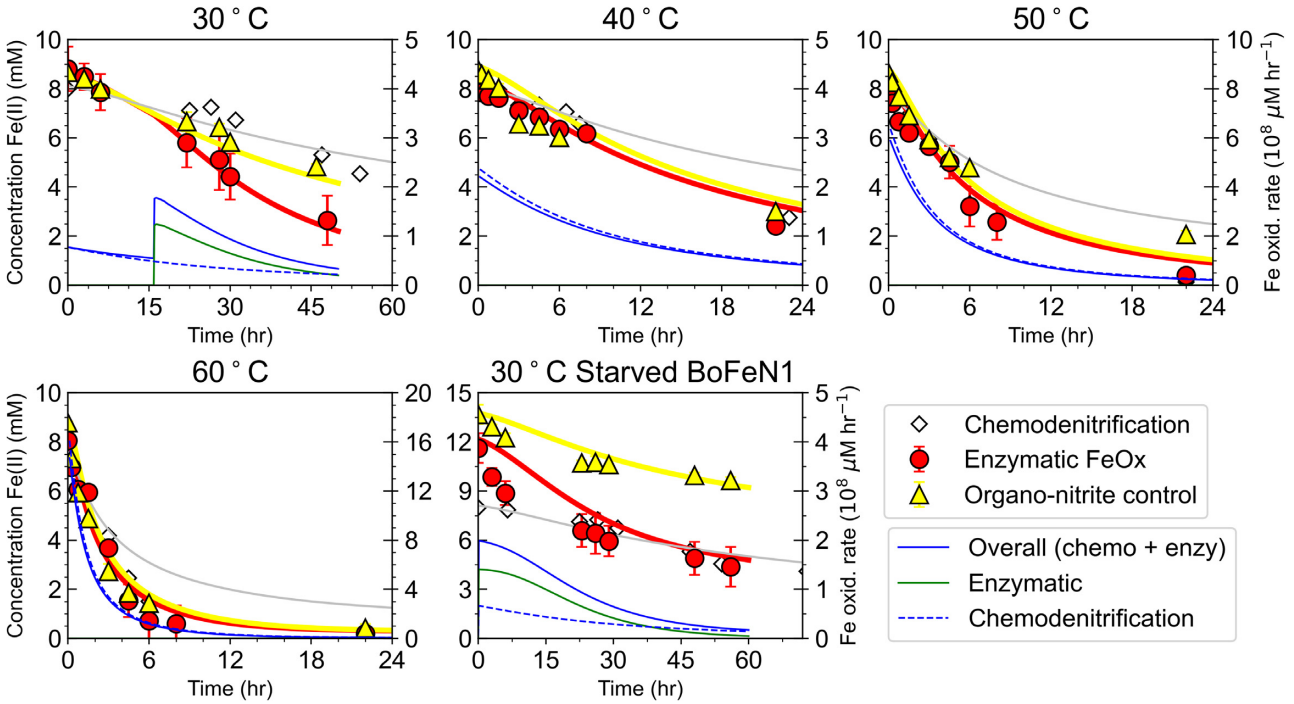

Figure 6. Total Fe(II) concentration in enzymatic temperature dependent Fe(II) oxidation experiments over time for *Acidovorax* strain BoFeN1. Initially cultivated in Fe(II)-containing, pre-filtered medium with 10 mM nitrate and 5 mM acetate. Symbols represent the measured data and solid lines represent the model results. To illustrate the contribution of different oxidation processes over time the enzymatic Fe(II) oxidation rate, the Fe(II) oxidation rate within the organo-nitrite control experiments (i.e. chemodenitrification) and the overall Fe(II) oxidation rate are provided. For experiments at 40, 50 and 60°C the biological Fe(II) oxidation rate is zero as the strain is not metabolically active. The 30°C starved experimental setup depicts the addition of Fe(II) after growth of BoFeN1 for 10–14 days at 13åC with nitrate plus acetate (medium was not pre-filtered). Every symbol represents an independent experiment with triplicates and error bars are the standard deviation.

The observed Fe(II) oxidation kinetics indicated an initial slight lag phase before the onset of oxidation. This autocatalytic process was documented by Tai & Dempsey (2009) for Fe(II) oxidation by nitrite in the presence of hydrous ferric oxide and others who investigated the oxidation rates between homogenous and heterogenous solutions (Jones *et al.* 2015). Siderite and vivianite have been known to precipitate within this culture medium upon the addition of Fe(II) (Hohmann *et al.* 2010). Assuming siderite does precipitate within this medium, and that the rate of siderite oxidation by nitrite in our study was similar to what was determined for higher siderite concentrations (Rakshit, Matocha and Coyne 2008), the rate is significantly below the much faster reaction of Fe^{2+}_{diss} oxidation by nitrite (Tai and Dempsey 2009). For example, using the k_{obs} determined within each of the studies mentioned above, the apparent oxidation rates for 1 mM of Fe(II) either as siderite or $Fe^{2+}_{diss,}$ (in the presence of hydrous ferric oxides and 0.25 mM nitrite) are 1.38×10^{-4} and 4.33×10^{-3} mM hr^{-1}, respectively. The observed oxidation rate for Fe^{2+}_{diss} is about 30 times higher than for siderite. Consequently, the impact of siderite oxidation by nitrite on the overall total Fe(II) oxidation kinetics can safely be assumed to be negligible compared to Fe^{2+}_{diss} oxidation.

Influence of temperature on BoFeN1 growth characteristics and Fe(II) oxidation

The *Acidovorax* strain BoFeN1 has been shown to grow even at temperatures as low as 5°C. It may be assumed that this psychrotrophic capability is a physiological advantage that might be attributed to the location of its original isolation, Lake Constance, where water temperatures can fluctuate seasonally between 4 and 24°C. Upon cultivation at 5°C, BoFeN1 experienced robust growth, although distinct differences were apparent compared to cultivations at 28°C. During incubation with nitrate, acetate and Fe(II), acetate consumption was slow and nitrite accumulated to significantly higher concentrations (4 mM at 5°C in comparison to 1 mM at 28°C), in addition to a longer lag time (Fig. 3). Higher nitrite accumulation at lower temperatures is a common phenomenon in denitrifying communities (Dorland & Beauchamp 1991; Gomez, Gonzalez-Lopez and De La Rua 2009). It has previously been suggested that this could be caused by an unbalanced nitrate/nitrite reduction due to a differing temperature sensitivity of the enzymatic denitrification step (Betlach & Tiedje 1981; Saleh-Lakha *et al.* 2009). While cultivating BoFeN1 at 5°C in the presence of Fe(II), we observed negligible Fe(II) oxidation over the entire experimental period, although the strain was able to reduce nitrate and consume acetate. The limited oxidation of Fe(II) at 5°C may have several explanations. For example, Fe(II) oxidation may have largely resulted from the abiotic oxidation of the accumulated nitrite, which, as mentioned earlier, is extremely slow at 5°C. A stepwise utilization of acetate, and subsequent Fe(II) oxidation, as described by Kappler, Schink and Newman (2005) could have led to a significantly delayed start of Fe(II) oxidation, which was never reached in our experiments. BoFeN1 might only be able to couple Fe(II) oxidation to nitrate reduction above a specific threshold temperature. Below this threshold, decreased efficiencies and affinities of transport proteins might limit active Fe(II) uptake (Panoff *et al.* 1998; Nedwell 1999; Beales 2004). If active Fe(II) transport into the periplasm is needed, changes in temperature could lead to a

reduced availability and oxidation. Finally, it is also possible that the involved enzyme, probably a c-type cytochrome, is not or significantly less active at lower temperatures. Shi et al., purified the cytochromes OmcA and MtrC, which are involved in electron transfer during Fe(III) reduction in *Shewanella* oneidensis MR-1, and they observed high activity at 25°C but no activity at 4°C (Shi *et al.* 2006). Still, there are several examples of acidophilic, microaerophilic Fe(II)-oxidizing strains and also environmental communities where Fe(II) oxidation is possible over a wide temperature range, without loss of Fe(II) oxidation activity at low temperatures in both fresh and marine waters (Ferroni, Leduc and Todd 1986; Ahonen & Tuovinen 1989; Cockell *et al.* 2011; Vollrath *et al.* 2013).

Comparison of enzymatic Fe(II) oxidation and chemodenitrification rates

Due to numerous competing processes removing total Fe(II) from solution, a meaningful comparison of oxidation rates between temperature dependent: enzymatic Fe(II) oxidation, organo-nitrite controls, and chemodenitrification experiments (Fig. 1) was not immediately possible from the visual inspection of the measured data alone. However, the model-based interpretation can quantify the contributions of these interdependent, competing processes on overall Fe(II) oxidation.

For enzymatic Fe(II) oxidation experiments and organo-nitrite controls at 40, 50 and 60°C, where BoFeN1 is inactive, the k_{app} observed were similar to the k_{app} determined for the chemodenitrification experiments, due to the absent contribution of biological Fe(II) oxidation and/or production of additional nitrite (Fig. 4; Table S1, Supporting Information). These results (Fig. 2) were reproduced in the biogeochemical modeling where either no or negligible amounts of additional nitrite were produced and no biological oxidation of Fe(II) occurred as the maximum temperature where growth can still occur was set at 37°C, consistent with previously reported data on the ecophysiology of strain BoFeN1 (Muehe *et al.* 2009).

The dynamics of the Fe(II) oxidation rates at temperatures of 30–60°C were different between the enzymatic Fe(II) oxidation and organo-nitrite control experiments (Fig. 6). Firstly, no lag phase was observed for the enzymatic Fe(II) oxidation experiments at any of the investigated temperatures, in contrast to what was observed in the chemodenitrification and organo-nitrite control experiments. This lag phase is most noticeable in the chemodenitrification experiments conducted at 5°C temperature, where little oxidation was observed at any of the three nitrite concentrations used for the first 10 days (Fig. 2). Conversely, in the enzymatic Fe(II) oxidation experiments the observed oxidation was almost immediate after the addition of Fe(II) and nitrite before slowing down as the reactant concentrations diminished. This result is counterintuitive as it would be expected for the experiment at 30°C, for example, that after a temperature change of 25°C (incubation performed at 5°C), combined with a possible Fe(II) toxicity effect (Bird, Coleman and Newman 2013), the bacteria would require at least a brief adaptation period prior to generating a high metabolic activity.

At 30°C we observed higher Fe(II) oxidation rates for the enzymatic Fe(II) oxidation experiments versus the organo-nitrite controls and chemodenitrification experiments. This temperature is close to the optimum temperature for biological growth for strain BoFeN1 and therefore any processes dependent on biological activity are enhanced. Fig. 6 shows a strong contribution of biological oxidation to the overall Fe(II) oxidation rate (at 30°C)

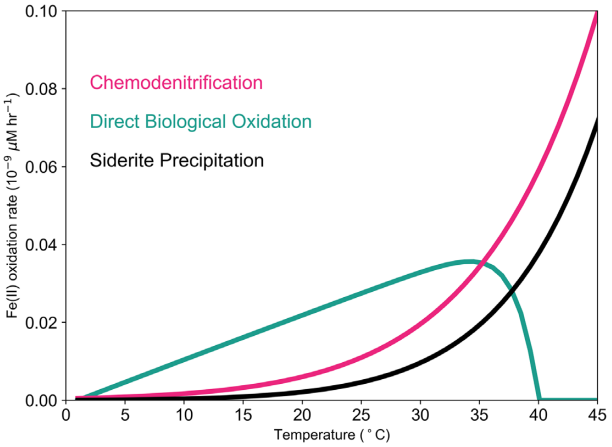

Figure 7. Rates of chemodenitrification and direct biological oxidation across a temperature range of 0 to 45°C and assuming 50 μM of NO_2^-, 200 μM of NO_3^- and 1 mM of Fe(II) is present in a 1 mM HCO_3^- solution (ionic strength = 0.01 M) with an initial biomass concentration of ~1.5×10^6 cells mL^{-1} (a factor of 10^{-13} g cell^{-1} was used to convert from cells mL^{-1} to mol L^{-1} using the formula for biomass given a generic formula of $C_5H_7O_2N$).

before all nitrate is consumed. Modeling estimated the overall contribution of chemodenitrification at 30°C to be 26%, significantly less than what was calculated for the higher temperatures 40°, 50° and 60°C which were all greater than 94%. The contribution of chemodenitrification at 30°C was similar to the 35% quantified by Jamieson *et al.* (2018). Across the more environmentally relevant temperature range of 5–30°C where strain BoFeN1 is known to be active, simulated results for the contribution of chemodenitrification to overall Fe(II) oxidation remained reasonably consistent between 19% and 29%. This demonstrates biological oxidation of Fe(II) consistently contributes to overall Fe(II) oxidation up until the temperature reaches the upper limit of bacterial growth.

Using the biogeochemical model, the oxidation rates of chemodenitrification and enzymatic Fe(II) oxidation were evaluated across the temperature range from 5–45°C, assuming 50 μM of NO_2^- and 200 μM of NO_3^-, 1 mM of Fe(II) as an electron donor and a biomass concentration of ~1.5×10^6 cells mL^{-1}. Fig. 7 shows that under these conditions the enzymatic Fe(II) oxidation rate is significantly greater than the chemodenitrification rate across 0–30°C, and is the primary process responsible for Fe(II) oxidation across this temperature range. Collecting more experimental data on Fe(II) oxidation rates within batch cultures or within a continuous-flow setup, using environmentally relevant concentrations of Fe(II) and NO_3^- (e.g. micromolar concentrations) as well as several other strains would be useful to better determine the contribution of abiotic and biotic Fe(II) oxidation in the natural environment. Further, performing these experiments at temperatures within either ends of the spectrum where bacterial growth is still possible would also provide insight into how the contribution from each of these processes can change across seasons within soil and sedimentary environments.

Starving the cells of acetate and internal stored carbon yielded similar results, with higher observed Fe(II) oxidation rates measured in enzymatic Fe(II) oxidation cultures compared to organo-nitrite controls (Fig. 6). These observations were again generally matched by the model simulations. We assume that there are combined effects of a) direct enzymatic/biological Fe(II) oxidation, which is assumed to begin immediately as no acetate is present to act as a primary electron donor (Fig. 6), and B) the

subsequent additional Fe(II) oxidation, that occurs due to production of nitrite from the former reaction. Additional electron donating capacity may have been provided by organic matter released from dying cells, although the extent of cannibalistic behavior is not known for this specific strain. Using alternative options to inactivate the cells without cell lysis, e.g. with biocides, was not feasible because of the high reactivity of nitrite towards these chemicals.

Mineral formation

During both the abiotic and biotic incubations, we observed an initial formation of green rust, as well as some poorly crystalline-ferrihydrite-type Fe(III) oxyhydroxides, and a terminal mineral phase of goethite (Pantke *et al.* 2012). This observation is consistent with earlier studies (Hansen, Borggaard and Sorensen 1994; Kampschreur *et al.* 2011), that similarly observed an initial green rust formation during Fe(II) oxidation by nitrite, followed by a transformation to goethite. A striking feature was the observed hexagonal structure of the minerals while forming at higher temperatures, especially at 60°C. While this is the typical crystal structure of green rust (McGill, McEnaney and Smith 1976), it was maintained during and after the transformation to goethite (Fig. 5). Mineral encrustation of BoFeN1 cells was previously described to appear in the common needle- or globular-like structure (Pantke *et al.* 2012; Miot *et al.* 2011). This was also visible in our experiments at all temperatures, with more needle-like goethite at higher temperatures and more globular goethite at lower temperatures (Fig. 5), indicating that encrustation may be abiotically driven by Fe(II) sorption to the cells and subsequent oxidation by nitrite (Coby and Picardal 2005; Klueglein and Kappler 2013).

CONCLUSIONS

Our experimental data and the corresponding process-based model simulations demonstrate that the reaction between nitrite and Fe(II) significantly contributes to overall Fe(II) oxidation at circumneutral pH, with the contribution increasing as the temperature increases due to the typical Arrhenius-type behavior of this abiotic oxidation reaction. At temperatures above 40°C this Fe(II)-oxidizing strain is no longer metabolically active and chemodenitrification becomes the sole process responsible for overall Fe(II) oxidation. *Acidovorax* strain BoFeN1 oxidizes Fe(II) very slowly at low temperatures, although some growth is possible. However, increased Fe(II) oxidation rates observed at 30°C, when cells but no acetate were present, indicate direct enzymatic Fe(II) oxidation by the bacteria was occurring. Consequently, if we assume similar Fe(II) oxidation pathways for strains or enrichments capable of chemolithoautotrophic growth, then these bacteria retain their growth advantage for using Fe(II) as an electron donor across typical environmental temperature ranges. This strengthens the growing amount of evidence demonstrating the potential importance of these bacteria in overall Fe cycling.

Future experiments with a completely different Fe(II)-oxidizer might help to understand general (and not only strain-specific) temperature effects. Assuming direct enzymatic nitrate-dependent Fe(II) oxidation is possible, the cells must compete with the abiotic oxidation of Fe(II) by nitrite, similar to the competition between microaerophilic Fe(II)-oxidizing bacteria with the abiotic oxidation of Fe(II) by oxygen. Strategies for how different bacteria could deal with this competition between biotic and abiotic Fe(II) oxidation in the environment have yet to be determined.

SUPPLEMENTARY DATA

Supplementary data are available at *FEMSEC* online.

FUNDING

This work was funded by infrastructural support by the DFG under Germany's Excellence Strategy, cluster of Excellence EXC2124, project ID 390838134 and the US Department of Energy, Grant Number DE-EE0009506.

ACKNOWLEDGEMENTS

We want to thank Tina Gauger and Katja Laufer for their ideas and helpful discussions on this topic. Also, we want to thank Ellen Röhm for acetate and NO_x measurements and Nikolas Hagemann for SEM imaging. James Byrne and Christoph Berthold are acknowledged for XRD analyses.

Conflict of interest. None declared.

REFERENCES

Ahonen L, Tuovinen OH. Microbial oxidation of ferrous iron at low-temperatures. *Appl Environ Microbiol* 1989;**55**:312–6.

Beales N. Adaptation of microorganisms to cold temperatures, weak acid preservatives, low pH, and osmotic stress: a review. *Comprehensive Reviews in Food Science and Food Safety* 2004;**3**:1–20.

Beller HR, Zhou P, Legler TC *et al.* Genome-enabled studies of anaerobic, nitrate-dependent iron oxidation in the chemolithoautotrophic bacterium Thiobacillus denitrificans. *Frontiers in Microbiology* 2013;**4**.

Benz M, Brune A, Schink B. Anaerobic and aerobic oxidation of ferrous iron at neutral pH by chemoheterotrophic nitrate-reducing bacteria. *Arch Microbiol* 1998;**169**:159–65.

Betlach MR, Tiedje JM. Kinetic explanation for accumulation of nitrite, nitric-oxide, and nitrous-oxide during bacterial denitrification. *Appl Environ Microbiol* 1981;**42**:1074–84.

Bird LJ, Coleman ML, Newman DK. Iron and copper act synergistically to delay anaerobic growth of bacteria. *Appl Environ Microbiol* 2013;**79**:3619–27.

Blöthe M, Roden EE. Composition and Activity of an Autotrophic Fe(II)-Oxidizing, Nitrate-Reducing Enrichment Culture. *Appl Environ Microbiol* 2009;**75**:6937–40.

Bonner FT, Pearsall KA. Aqueous Nitrosyliron(I1) Chemistry. 1. Reduction of Nitrite and Nitric Oxide by Iron(I1) and (Trioxodinitrato)iron(II) in Acetate Buffer. Intermediacy of Nitrosyl Hydride. *Inorg Chem* 1982;**21**:1973–8.

Borch T, Kretzschmar R, Kappler A *et al.* Biogeochemical redox processes and their impact on contaminant dynamics. *Environ Sci Technol* 2010;**44**:15–23.

Bryce C, Blackwell N, Schmidt C *et al.* Microbial anaerobic Fe (II) oxidation–Ecology, mechanisms and environmental implications. *Environ Microbiol* 2018;**20**:3462–83.

Carlson HK, Clark IC, Blazewicz SJ *et al.* Fe(II) oxidation is an innate capability of nitrate-reducing bacteria that involves abiotic and biotic reactions. *J Bacteriol* 2013;**195**:3260–8.

Chakraborty A, Picardal F. Induction of nitrate-dependent Fe(II) oxidation by Fe(II) in *Dechloromonas* sp strain UWNR4 and

Acidovorax sp strain 2AN. *Appl Environ Microbiol* 2013;**79**: 748–52.

Coby AJ, Picardal FW. Inhibition of NO3- and NO2- reduction by microbial Fe(III) reduction: evidence of a reaction between NO2- and cell surface-bound Fe2+. *Appl Environ Microbiol* 2005;**71**:5267–74.

Cockell CS, Kelly LC, Summers S *et al.* Following the Kinetics: iron-Oxidizing Microbial Mats in Cold Icelandic Volcanic Habitats and Their Rock-Associated Carbonaceous Signature. *Astrobiology* 2011;**11**:679–94.

Dorland S, Beauchamp E. Denitrification and ammonification at low soil temperatures. *Can J Soil Sci* 1991;**71**: 293–303.

Etique M, Jorand FdrP, Zegeye A *et al.* Abiotic process for Fe (II) oxidation and green rust mineralization driven by a heterotrophic nitrate reducing bacteria (Klebsiella mobilis). *Environ Sci Technol* 2014;**48**:3742–51.

Ferroni GD, Leduc LG, Todd M. Isolation and temperature characterization of psychrotrophic strains of *Thiobacillus ferrooxidans* from the environment of a uranium mine. *J Gen Appl Microbiol* 1986;**32**:169–75.

Gomez MA, Gonzalez-Lopez J, De La Rua A. Effect of temperature over start-up of a groundwater-denitrifying submerged filter inoculated with psychrotolerant bacteria. *Journal of Environmental Science and Health Part a-Toxic/Hazardous Substances & Environmental Engineering* 2009;**44**:1298–305.

Greenberg J, Tomson M. Precipitation and dissolution kinetics and equilibria of aqueous ferrous carbonate vs temperature. *Appl Geochem* 1992;**7**:185–90.

Hansen H, Koch CB. Reduction of nitrate to ammonium by sulphate green rust; activation energy and reaction mechanism. *Clay Miner* 1998;**33**:87–101.

Hansen HCB, Borggaard OK, Sorensen J. Evaluation of the free-energy of formation of Fe(II)-Fe(III) hydroxide-sulfate (green rust) and its reduction by nitrite. *Geochim Cosmochim Acta* 1994;**58**:2599–608.

Hansen HCB, Koch CB, Nancke-Krogh H *et al.* Abiotic nitrate reduction to ammonium: key role of green rust. *Environ Sci Technol* 1996;**30**:2053–6.

He S, Tominski C, Kappler A *et al.* Metagenomic analyses of the autotrophic Fe (II)-oxidizing, nitrate-reducing enrichment culture KS. *Appl Environ Microbiol* 2016;**82**: 2656–68.

Hedrich S, Schlomann M, Johnson DB. The iron-oxidizing proteobacteria. *Microbiology* 2011;**157**:1551–64.

Hegler F, Schmidt C, Schwarz H *et al.* Does a low-pH microenvironment around phototrophic FeII-oxidizing bacteria prevent cell encrustation by FeIII minerals? *FEMS Microbiol Ecol* 2010;**74**:592–600.

Hinkle MAG, Wang Z, Giammar DE *et al.* Interaction of Fe(II) with phosphate and sulfate on iron oxide surfaces. *Geochim Cosmochim Acta* 2015;**158**:130–46.

Hohmann C, Winkler E, Morin G *et al.* Anaerobic Fe(II)-Oxidizing Bacteria Show As Resistance and Immobilize As during Fe(III) Mineral Precipitation. *Environ Sci Technol* 2010;**44**: 94–101.

Huang YM, Straub D, Kappler A *et al.* A Novel Enrichment Culture Highlights Core Features of Microbial Networks Contributing to Autotrophic Fe(II) Oxidation Coupled to Nitrate Reduction. *Microbial Physiology* 2021;**31**.

Jakus N, Blackwell N, Osenbrück K *et al.* Nitrate Removal by a Novel Lithoautotrophic Nitrate-Reducing, Iron(II)-Oxidizing Culture Enriched from a Pyrite-Rich Limestone Aquifer. *Appl Environ Microbiol* 2021;**87**:e00460–00421.

Jamieson J, Prommer H, Kaksonen AH *et al.* Identifying and quantifying the intermediate processes during nitrate-dependent iron (II) oxidation. *Environ Sci Technol* 2018;**52**:5771–81.

Jiang CZ, Tosca NJ. Growth kinetics of siderite at 298.15 K and 1 bar. *Geochim Cosmochim Acta* 2020;**274**:97–117.

Jin Q, Bethke CM. A new rate law describing microbial respiration. *Appl Environ Microbiol* 2003;**69**:2340–8.

Jones LC, Peters B, Lezama Pacheco JS *et al.* Stable isotopes and iron oxide mineral products as markers of chemodenitrification. *Environ Sci Technol* 2015;**49**:3444–52.

Kampschreur MJ, Kleerebezem R, de Vet W *et al.* Reduced iron induced nitric oxide and nitrous oxide emission. *Water Res* 2011;**45**:5945–52.

Kappler A, Bryce C, Mansor M *et al.* An evolving view on biogeochemical cycling of iron. *Nat Rev Microbiol* 2021;1–15.

Kappler A, Newman DK. Formation of Fe(III)-minerals by Fe(II)-oxidizing photoautotrophic bacteria. *Geochim Cosmochim Acta* 2004;**68**:1217–26.

Kappler A, Schink B, Newman DK. Fe(III) mineral formation and cell encrustation by the nitrate-dependent Fe(II)-oxidizer strain BoFeN1. *Geobiology* 2005;**3**:235–45.

Kappler A, Straub KL. Geomicrobiological cycling of iron. *Molecular Geomicrobiology* 2005;**59**:85–108.

Kendall B, Anbar AD, Kappler A *et al.* The global iron cycle. *Fundamentals of Geobiology*. Hoboken, New Jersey: John Wiley & Sons, Ltd, 2012, 65–92.

Klueglein N, Kappler A. Abiotic oxidation of Fe(II) by reactive nitrogen species in cultures of the nitrate-reducing Fe(II) oxidizer *Acidovorax* sp. BoFeN1 – questioning the existence of enzymatic Fe(II) oxidation. *Geobiology* 2013;**11**:180–90.

Kopf SH, Henny C, Newman DK. Ligand-enhanced abiotic iron oxidation and the effects of chemical versus biological iron cycling in anoxic environments. *Environ Sci Technol* 2013;**47**: 2602–11.

Laidler KJ. The development of the Arrhenius equation. *J Chem Educ* 1984;**61**:494.

Laufer K, Røy H, Jørgensen BB *et al.* Evidence for the existence of autotrophic nitrate-reducing Fe (II)-oxidizing bacteria in marine coastal sediment. *Appl Environ Microbiol* 2016;**82**:6120–31.

Liu T, Chen D, Luo X *et al.* Microbially mediated nitrate-reducing Fe(II) oxidation: quantification of chemodenitrification and biological reactions. *Geochim Cosmochim Acta* 2019;**256**: 97–115.

Mathur SS, Dzombak DA. Chapter 16 - Surface complexation modeling: goethite. *Interface Science and Technology*.**Vol. 11**, Lützenkirchen J (ed). Elsevier, 2006, 443–68.

McGill I, McEnaney B, Smith D. Crystal structure of green rust formed by corrosion of cast iron. 1976.

Miot J, Maclellan K, Benzerara K *et al.* Preservation of protein globules and peptidoglycan in the mineralized cell wall of nitrate-reducing, iron(II)-oxidizing bacteria: a cryo-electron microscopy study. *Geobiology* 2011;**9**:459–70.

Muehe EM, Gerhardt S, Schink B *et al.* Ecophysiology and the energetic benefit of mixotrophic Fe(II) oxidation by various strains of nitrate-reducing bacteria. *FEMS Microbiol Ecol* 2009;**70**:335–43.

Nedwell D. Effect of low temperature on microbial growth: lowered affinity for substrates limits growth at low temperature. *FEMS Microbiol Ecol* 1999;**30**:101–11.

Notini L, Byrne JM, Tomaszewski EJ *et al.* Mineral Defects Enhance Bioavailability of Goethite toward Microbial Fe(III) Reduction. *Environmental Science & Technology* 2019;**53**: 8883–91.

Palandri J, Kharaka Y. A Compilation of Rate Parameters of Water-Mineral Interaction Kinetics for Application to Geochemical Modeling. *U.S. Geological Survey Open File Report* 2004;**1068**:71.

Panoff J-M, Thammavongs B, Guéguen M *et al.* Cold stress responses in mesophilic bacteria. *Cryobiology* 1998;**36**:75–83.

Pantke C, Obst M, Benzerara K *et al.* Green rust formation during Fe (II) oxidation by the nitrate-reducing Acidovorax sp. strain BoFeN1. *Environ Sci Technol* 2012;**46**:1439–46.

Parkhurst DL, Appelo C. *Description of input and examples for PHREEQC version 3: a computer program for speciation, batch-reaction, one-dimensional transport, and inverse geochemical calculations*. US Geological Survey, 2013.

Pokrovsky OS, Schott J. Surface Chemistry and Dissolution Kinetics of Divalent Metal Carbonates. *Environ Sci Technol* 2002;**36**:426–32.

Rakshit S, Matocha CJ, Coyne MS. Nitrite Reduction by Siderite. *Soil Sci Soc Am J* 2008;**72**:1070–7.

Ratkowsky D, Olley J, McMeekin T *et al.* Relationship between temperature and growth rate of bacterial cultures. *J Bacteriol* 1982;**149**:1–5.

Saleh-Lakha S, Shannon KE, Henderson SL *et al.* Effect of pH and temperature on denitrification gene expression and activity in Pseudomonas mandelii. *Appl Environ Microbiol* 2009;**75**:3903–11.

Schaedler F, Kappler A, Schmidt C. A revised iron extraction protocol for environmental samples rich in nitrite and carbonate. *Geomicrobiol J* 2018;**35**:23–30.

Shi L, Chen B, Wang Z *et al.* Isolation of a high-affinity functional protein complex between OmcA and MtrC: two outer membrane decaheme c-type cytochromes of Shewanella oneidensis MR-1. *J Bacteriol* 2006;**188**:4705–14.

Sorensen J, Thorling L. Stimulation by lepidocrocite (gamme-FeOOH) of Fe(II)-dependent nitrite reduction. *Geochim Cosmochim Acta* 1991;**55**:1289–94.

Straub KL, Benz M, Schink B *et al.* Anaerobic, nitrate-dependent microbial oxidation of ferrous iron. *Appl Environ Microbiol* 1996;**62**:1458–60.

Sun W, Nešic S. Kinetics of corrosion layer formation: part 1—iron carbonate layers in carbon dioxide corrosion. *Corrosion* 2008;**64**:334–46.

Tai YL, Dempsey BA. Nitrite reduction with hydrous ferric oxide and Fe(II): stoichiometry, rate, and mechanism. *Water Res* 2009;**43**:546–52.

Van Cappellen P, Charlet L, Stumm W *et al.* A surface complexation model of the carbonate mineral-aqueous solution interface. *Geochim Cosmochim Acta* 1993;**57**:3505–18.

Van Cleemput O, Baert L. Nitrite stability influenced by iron compounds. *Soil Biol Biochem* 1983;**15**:137–40.

Vollrath S, Behrends T, Koch CB *et al.* Effects of temperature on rates and mineral products of microbial Fe(II) oxidation by Leptothrix cholodnii at microaerobic conditions. *Geochim Cosmochim Acta* 2013;**108**:107–24.

Weber KA, Picardal FW, Roden EE. Microbially catalyzed nitrate-dependent oxidation of biogenic solid-phase Fe (II) compounds. *Environ Sci Technol* 2001;**35**:1644–50.

Weber KA, Pollock J, Cole KA *et al.* Anaerobic nitrate-dependent iron(II) bio-oxidation by a novel lithoautotrophic betaproteobacterium, strain 2002. *Appl Environ Microbiol* 2006;**72**:686–94.

Welter DE, White JT, Hunt RJ *et al. Approaches in highly parameterized inversion—PEST++ Version 3, a Parameter ESTimation and uncertainty analysis software suite optimized for large environmental models*. Reston, VA, 2015, 64.